TUS

JOURNAL OF GEOPHYSICAL RESEARCH, VOL. 104, NO. D2, PAGES 2015–2030, JANUARY 27, 1999

Reassessment of the moisture source over the Sahara Desert based on NASA reanalysis

Y. Shay-El and P. Alpert
Department of Geophysics and Planetary Sciences, Tel Aviv University, Israel

A. da Silva
Data Assimilation Office, NASA/GSFC, Greenbelt, Maryland

Abstract. The components of the moisture balance equation are calculated for the Middle East/North Africa regions based on NASA/GEOS-1 multiyear reanalysis data set. These include the Evaporation (E), Precipitation (P), moisture flux divergence ($\nabla \cdot \mathbf{Q}$), and errors associated with the incremental analysis updates of the specific humidity, or IAU(q). The Annual mean $\nabla \cdot \mathbf{Q}$ corresponds well to the results of *Vitart et al.* [1996], based on NCEP data. IAU(q) reveals a strong moisture source over the eastern Mediterranean and also confirms the paradoxical net moisture sink over the Arabian-Iraqi desert found by *Alpert and Shay-El* [1993]. Over the North African Sahara Desert the moisture flux was shown to converge through the northern and southern boundaries mainly at low levels (~900 hPa) and to diverge through the eastern and western boundaries at higher levels (~700 hPa). *Starr and Peixoto* [1958] have classified North Africa as a net moisture source. Area averaging of $\nabla \cdot \mathbf{Q}$ over a box with varying dimensions reveals that it can be classified as a net sink if the box is small enough and located over the center of the desert. If the box is big enough to include the boundaries of the continent only then can it be classified as net source or divergence zone. Inspection of the intermonthly and diurnal variability, as well as the model biases, weakens also the net source argument. It is suggested that the earlier finding of a net source might be due to the smoothing of the water/land boundary, or due to various atmospheric diffusion processes such as the sea breeze cycle and cloud intrusion and evaporation.

1. Introduction

Climate studies of the hydrological cycle are frequently based on the estimation of the terms of the moisture balance equation using observations of the moisture-related fields. In particular, a common assumption is that the vertically integrated moisture flux divergence, $\nabla \cdot \mathbf{Q}$, is equal to the evaporation minus precipitation ($E - P$), which is then interpreted as the ground runoff [e.g., *Peixoto and Oort*, 1992]. Many studies have emphasized the large uncertainties involved in estimation of the atmospheric moisture budget terms [*Wang and Paegle*, 1996; *Rasmusson et al.*, 1996; *Trenberth and Guillemot*, 1995, 1998]. These uncertainties are related both to insufficient observations and to inadequate or missing representation of the physical moisture processes. They may have crucial impact on the evaluation of the budget over data sparse and water sparse arid regions, such as in the Middle East/North Africa [*Alpert et al.*, 1996]. The purpose of this paper is to reexamine thoroughly the moisture balance in these regions, using the state of the art data bases created by modern assimilation techniques, such as NASA/GEOS-1 reanalysis data set. Results will be compared to other studies in these regions, employing National Centers for Environmental Prediction (NCEP) data [e.g., *Vitart et al.*, 1996], and to other data sets such as GPCP [*Huffman et al.*, 1997].

On average, evaporation (E) in the subtropics is much larger than precipitation (P) [*Oort and Peixoto*, 1983]. The moisture excess is continuously transported by the atmospheric circulation systems both to the midlatitudes and largely to the tropics, where it is condensed and forms the precipitation in these precipitation belts. Over the continental subtropics, however, E and P are presumably very small, due to both the lack of surface water source and the subsidence. An exception to this was the finding of a paradoxical net moisture sink, or negative $\nabla \cdot \mathbf{Q}$, over the Arabian-Iraqi desert during winter. This feature was first noted by *Alpert and Shay-El* [1993] who used 6 years of operational European Center for Medium-Range Weather Forecasts (ECMWF) analysis data. Since this desert region has very scarce rainfall, the excess of precipitation over evaporation as a possible explanation can be easily ruled out. The probable scenario suggested was that cloud condensation exceeds evaporation but is not compensated by rainfall at the surface. Frequent medium- and high-level clouds which develop in this region are horizontally advected out of the region by the prevailing subtropical jet, removing in the form of cloud droplets the water vapor which converged to this region. Recently, Y. Shay-El et al. (unpublished data, 1998) have evaluated the cloud liquid water (CLW) flux employing satellite data (ISCCP and SSMI) and NASA/GEOS-1 reanalysis data sets. They have found divergence of CLW flux over the Arabian-Iraqi regions opposing in sign the vapor convergence but in smaller magnitude, thus at least partly confirming the above scenario. The divergence of CLW fluxes was also suggested to be important over warm ocean currents [*Peixoto*, 1973]. These divergences are generally ignored in moisture budgets calculations.

Paper number 1998JD200003.
0148-0227/99/1998JD200003$09.00

Another subtropical moisture paradox is the net source over the North African Sahara Desert, found by *Starr and Peixoto* [1958], *Peixoto* [1960] and, recently, further investigated by *Alpert and Shay-El* [1993], Y. Shay-El et al. (1998), and *Vitart et al.* [1996]. One explanation for this apparent domination of evaporation over precipitation, suggested by *Peixoto* [1960], is through the supply of water by surface and underground flow from less arid areas. A second explanation, suggested by *Shay-El and Alpert* [1991], is the evaporation of clouds intruding from the surrounding water bodies. This was partly supported by convergence of CLW over the northern part and the southwestern part of the Sahara (Y. Shay-El et al., 1998). Yet, a third explanation, suggested by *Vitart et al.* [1996], is due to errors in the representation of the diurnal sea breeze cycle. The sea breeze, which is particularly strong over the subtropics [*Atkinson*, 1981], may be an agent for pumping significant quantities of moisture to the Sahara from the nearby large water bodies. This effect, of sub-grid scale, is known to be underestimated by large-scale data sets. *Wang and Paegle* [1996] have shown that another sub-grid-scale phenomenon, i.e., the low-level jet over North America, plays a crucial role in moisture transport, which was commonly neglected. Recent studies by *Helfand et al.* [1996] also confirmed this.

In addition, the large-scale data sets, which are frequently used for moisture budget calculation, are largely determined by the assimilation models which generate them. The models suffer from many deficiencies, leading to systematic errors or biases that strongly influence data sparse regions like the middle East and especially where the evaporation and precipitation are very small. *Dee and da Silva* [1998] have shown that these biases are not removed in the current version 1 of the NASA/GEOS data set, therefore the climate of the reanalysis is somewhat biased toward the model's climate.

In this paper we will discuss in some detail the above mentioned processes which cause uncertainties in the moisture budget over the North Africa/Middle East. The data and equations are introduced in section 2. The 8-year annual mean terms of the moisture balance are discussed in section 3. In section 4 the three-dimensional moisture transport fields are examined. The area-averaged moisture flux divergence over the Sahara Desert is investigated in section 5. In section 6 we discuss the seasonal and diurnal variability of the moisture budget, and errors due to model biases are evaluated as well. The summary and conclusions are given in section 7.

2. Data and Equations

The NASA/GEOS-1/DAS (NASA Goddard Earth Observing System data assimilation system, version 1) reanalysis data set, used extensively in this work, is produced by the Data Assimilation Office of NASA's Goddard Space Flight Center [*Schubert et al.*, 1993]. Parallel reanalysis efforts are being conducted at NCEP [*Kalnay et al.*, 1996] and ECMWF [*Gibson et al.*, 1994]. Besides eliminating spurious climatic signals arising from changes in the operational analysis system, reanalysis products include a wealth of diagnostic quantities which historically have not been made available with the operational products. Of particular interest for moisture budget studies and atmosphere/surface interactions are the estimates of moisture transports, precipitation, evaporation, and clouds, along with several boundary layer and convective diagnostic quantities. In this study we use 8 years of available data, from March 1985 to February 1993.

The vertically integrated moisture balance equation is commonly simplified to

$$\partial \bar{q}/\partial t + \nabla \cdot \bar{\mathbf{Q}} = \bar{E} - \bar{P} \tag{1}$$

where q is the vertically integrated specific humidity, Q is the horizontal transport vector of water vapor, and E and P are evaporation and precipitation, respectively. Overbar denotes time averaging. In the reanalysis these terms are accumulated every time step. We will use the multiyear annual and monthly means. The storage term $\partial \bar{q}/\partial t$ is normally small in climate studies, and the $E - P$ term is then assumed to balance the total column moisture divergence [e.g., *Shay-El and Alpert*, 1991].

In a data assimilation system, however, additional terms should be added to the moisture equation. Neglecting the storage term this reads

$$\nabla \cdot \bar{\mathbf{Q}} = \bar{E} - \bar{P} + \Delta + \text{filter} \tag{2}$$

where the term Δ, representing the correction to the model state by the observational data, is called the mean incremental analysis update (IAU); and filter includes the effects of the horizontal smoothing filter, such as the one suggested by *Shapiro* [1970] and being used in GEOS-1/DAS, and any filling of moisture to remove negative specific humidity. The IAU is computed from the differences in the specific humidity q between the analysis of humidity observations and the model short-term forecast (or first guess) and is inserted into the assimilation run as an additional forcing (for details, see *Bloom et al.* [1996]). This term compensates for biases in the estimates of $\nabla \cdot \mathbf{Q}$, $\bar{E}$ and $\bar{P}$, or any physical process not represented in the atmospheric general circulation model used in the assimilation system, such as the CLW flux divergence. It is also affected by biases in the observations. These, however, are assumed to be small in comparison with the other sources of errors, particularly over data scarce regions like those explored in the present study.

We will also use the three-dimensional moisture balance, without vertical integration. In this case, the equation is

$$\nabla_q \overline{\mathbf{V}} + \frac{\partial \overline{q\omega}}{\partial p} = \bar{S}_q \tag{3}$$

where S_q is the moisture net source, including the contributions of moist processes parameterizations of sub-grid and large-scale convection, cloud formation, precipitation and surface evaporation, as well as the vertical distribution of Δ and the filter.

3. Annual Mean Moisture Balance

Figure 1 depicts the 8-year annual mean terms of the vertically integrated moisture balance equation (equation (2)), using NASA/GEOS-1 data set, averaged for March 1985 to February 1993 over the Middle East/North Africa. The evaporation, precipitation, and their difference $E - P$, are shown in Figures 1a, 1b, and 1c, respectively. All units are in millimeters per day. These diagnostic fields are created by the model parameterizations with only indirect impact by observations. As expected, the evaporation maximized over water bodies and over the tropical central Africa, while low values close to zero are found over the North African Sahara Desert. The exact locations of the maxima over the Red Sea (~40°E, 10°–30°N) and the Persian Gulf (55°E, 27°N) are associated with

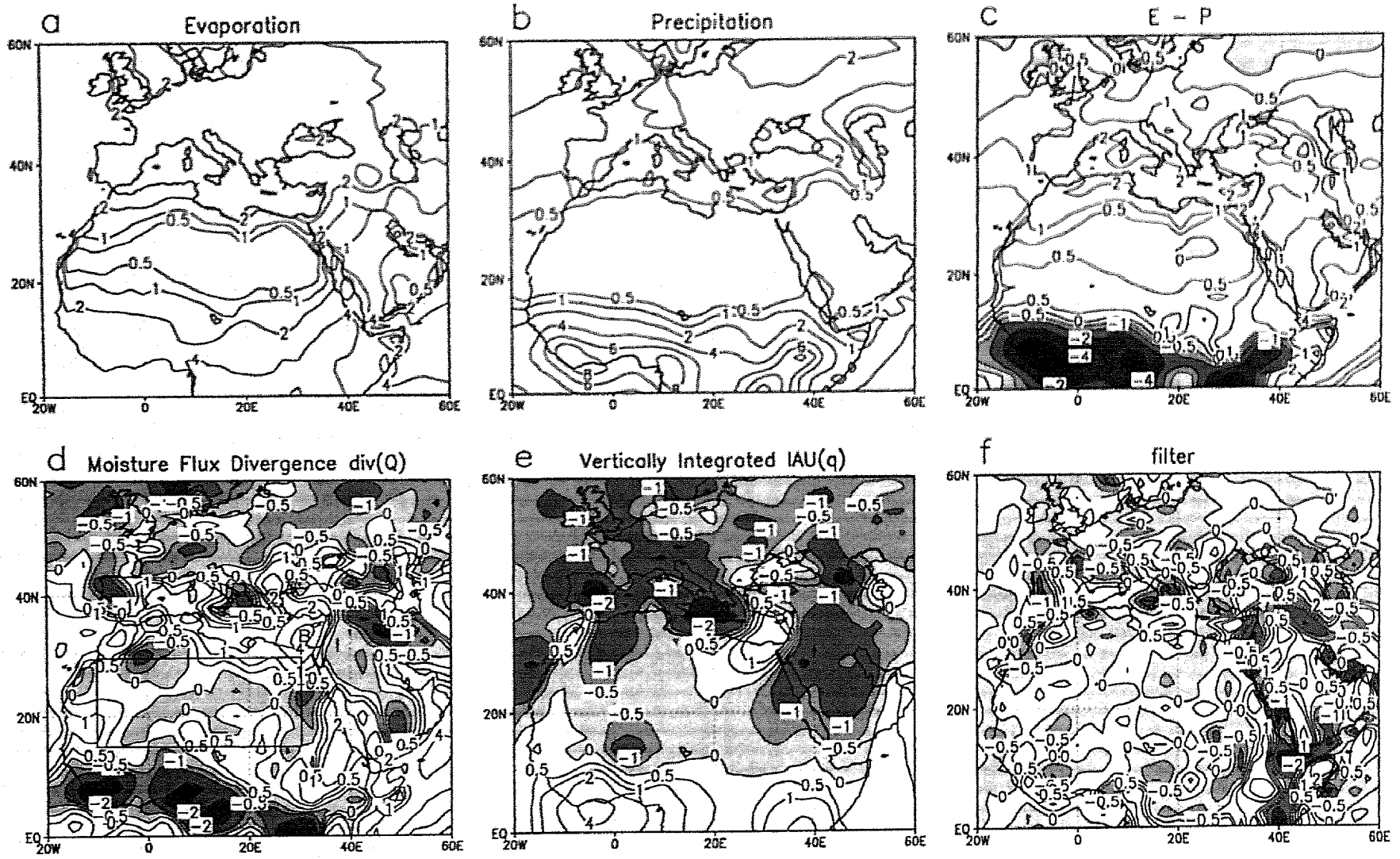

Figure 1. Eight-year annual mean components of the vertically integrated moisture balance, calculated from NASA/GEOS-1 data set, averaged from March 1985 to February 1993 over the Middle East/North Africa. (a) Evaporation, (b) precipitation, and (c) evaporation minus precipitation ($E - P$). (d) Moisture flux divergence $\nabla \cdot Q$. (e) incremental analysis updates for the specific humidity (IAU(q)) and (f) filter, estimated as a residual. All units are in millimeters per day (mm/d). Contour values are 0, ±0.5, ±1, ±2, ±4, ±6, ±8, and ±10 mm/d. Negative values are shaded. The Sahara study box (10°W–30°E : 15°N–30°N), following *Vitart et al.* [1996], is depicted in Figure 1d as well as the eastern Mediterranean point B (30°E, 32°N), which is further studied in reference to Figure 3b.

grid points defined as water using the land/water mask [see *Takacs et al.*, 1994, Figure 5]. The precipitation, Figure 1b, shows the two precipitation belts of the tropics (south of 20°N approximately) and the midlatitudes (north of 30°N approximately), while in between, there is the subtropical dry belt of almost no precipitation at all (less than 0.5 mm d^{-1}).

It is interesting to note that the positive evaporation pattern intrudes into the North African land more than the precipitation, resulting in positive $E - P$ over the Sahara Desert, as shown in Figure 1c. Therefore this confirms again the paradoxical moisture source from the desert surface mentioned above. However, the values of $E - P$ decrease as the distance increases away from the continental boundaries into land, leading even to negative values shown by the shaded close area around 25°E, 25°N, designating moisture sink. This can be interpreted as a gradual "diffusion" of water from the surrounding water bodies into the land. This water evaporates from the surface, thus being a source for the atmospheric moisture that does not precipitate but is advected out of the region (to be shown consequently). This scenario leads to the following question: Is this surface moisture diffusion real, or just a result of a smoothed water/land transition due to the low-resolution model and the lack of observations?

Some clues to this question might lie in the moist parameterizations of GEOS-1. On the basis of these parameterizations the surface evaporation is technically a function of the vertical gradient of moisture near the surface, the potential evapotranspiration fraction β, and the eddy exchange coefficient K_h [*Takacs et al.*, 1994]. It depends on the soil wetness climatology following *Schemm et al.* [1992]. Thus the smoothed water/land transition of the evaporation must depend to some extent on the presumed smoothed transition of these β and K_h parameters.

To avoid the dependency on the parameterizations, it is common to calculate the $E - P$ from the divergence of the vertically integrated moisture flux divergence $\nabla \cdot \mathbf{Q}$ and to assume, based on (1) (and by neglecting the storage term), that $\nabla \cdot \mathbf{Q}$ is equal to $E - P$. This method is sometimes referred to as the residual method. For instance, *Vitart et al.* [1996] calculated the moisture flux divergence based on NCEP reanalysis in order to study the hydrology, or $E - P$ patterns, of the North African desert. This method makes the preliminary assumption that Δ in (2) corrects only for inadequate physical parameterization of $E - P$ and not for errors in the dynamical $\nabla \cdot \mathbf{Q}$. This presumption might not be valid over regions with sparse observations and will be discussed later.

Figure 1d depicts the calculated annual mean $\nabla \cdot \mathbf{Q}$. Negative divergences are shaded. The overall picture over North Africa is similar to the "parameterized" Figure 1c, with positive values (interpreted as excess of evaporation over precipitation) over the water bodies surrounding the continent and overlapping it to some extent and negative values inside land. However, the areas of moisture convergence, or negative $\nabla \cdot \mathbf{Q}$, seem to be more extended, revealing some more regional details, as for example moisture convergence over the Atlas Mountains (0°E, 30°N). This figure agrees quite well with *Vitart et al.*'s [1996] Figure 3 (not shown here), showing also $\nabla \cdot \mathbf{Q}$ but as based on NCEP reanalysis.

Figure 1e shows the vertically integrated IAU(q) or Δ in (2), and Figure 1f shows the filter term which was estimated as a residual of the other terms following, for example, *Schubert et al.* [1995, p. 69]. The positive values of Δ over the tropics and negative over the midlatitudes are part of a global bias of the assimilation model toward excessive rainfall in the tropics and underestimated rainfall in the midlatitudes, as shown for example by *da Silva and White* [1995]. A regional opposite feature, however, is the positive Δ over the eastern Mediterranean. This might be associated with the strong evaporation over this region, as discussed by *Alpert and Shay-El* [1994], which might be underestimated by the model parameterization. For example, *Alpert et al.* [1997] have shown that evaporation for the Dead Sea reaches values of 1700–2000 mm/yr, equivalent to 5–6 mm/d. The local extreme dry climate of the Dead Sea may partly explain these very high evaporation values, but ~2 mm/d predicted by the model (Figure 1a) over the eastern Mediterranean are probably lower than necessary. Another optional explanation is that there are systematic errors in the humidity/wind data, such as biases in the estimation of the subsidence effects on the moisture field. In section 4 we will explore the vertical profiles of the moisture budget terms at the center of this large $\nabla \cdot \mathbf{Q}$.

The horizontal smoothing effect (Figure 1f) is shown, for example, to remove moisture from above the Red Sea (~40°E, 20°N) and to transfer it to its surrounding lands. While such a sub-grid moisture diffusion, from a sea area which is relatively rich in moisture to its surrounding moisture poor desert, is expected, it is a question to what extent this physical diffusion is accurately described by the model filtering. This point adds to the uncertainty of the water/land transition mentioned above and will be further discussed in section 5.

Another noticeable point is the relatively large negative Δ over the Arabian-Iraqi desert (~40°E, 30°N) associated with a negative mean $\nabla \cdot \mathbf{Q}$, or moisture convergence, over this region (Figure 1d), while $E - P$ is positive. This confirms again the paradoxical finding, by *Alpert and Shay-El* [1993] based on ECMWF operational data, of moisture convergence or sink over this desert region with very low precipitation. *Alpert and Shay-El* [1993] suggested that this converged moisture exits the region in the form of cloud liquid water. This scenario is further investigated by Y. Shay-El et al. (1998). *Trenberth and Guillemot* [1998] also noted this feature, based on NCEP reanalysis. They, however, associated it with excessive evaporation in the model. The inclusion of explicit CLW equations in the future version of GEOS will help to shed more light on this point.

4. Annual Mean Moisture Transport Fields

As discussed in section 3, one of the important tools for calculating moisture source/sinks is based on the assumption of its equality to the divergence of the moisture flux. Understanding the climate of the moisture transport by the atmospheric circulation is therefore essential for assessing the uncertainties in the resulting net source. Figure 2 shows the 8-year annual mean moisture transport vectors and divergence for the vertically integrated flux and for the 900 and 700 hPa isobaric levels as well. At the bottom panel of the figure the flux is depicted as streamlines. The vertically integrated streamlines, Figure 2d, reveal the anticyclonic subtropical cell over North Africa and another one over the Arabian Desert. Thus the moisture flux enters the Sahara Desert mainly from the northern boundary, i.e. from the Mediterranean and the Atlantic sources and partly from the Indian Ocean and from the Red Sea at the southeastern corner. It exits mainly through the southwestern corner via the central African easterlies. Only a small part of the flux is lost/gained over the Sahara Desert, as shown by the

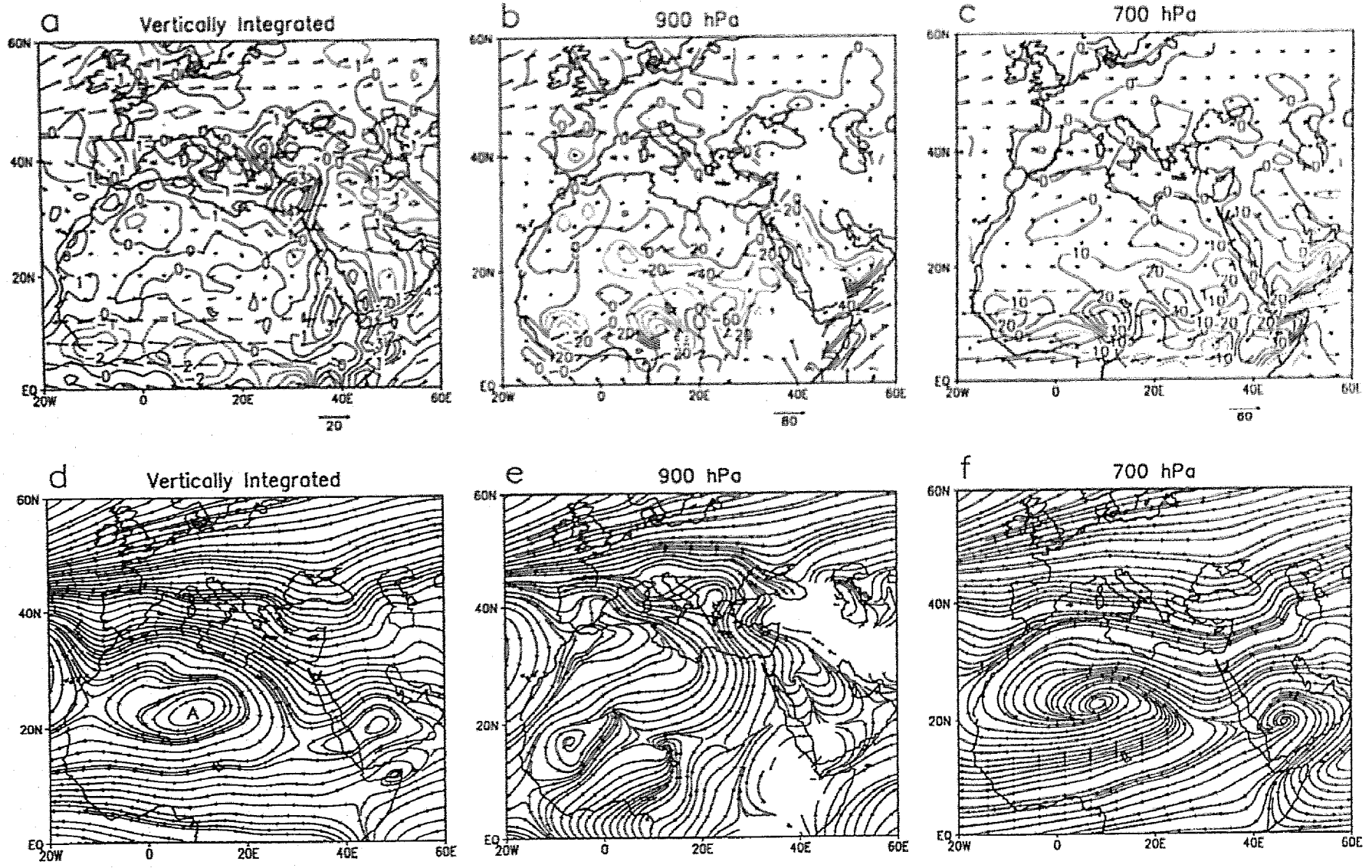

8yr Annual Moisture Flux, Divergence & Streamlines from NASA/GEOS-1

Figure 2. Eight-year annual mean moisture transport fields calculated from NASA/GEOS-1 data set: (a) vertically integrated moisture flux vectors, in units m/s g/kg, with every other vector skipped, and divergence contours (mm/d); (b) same as Figure 2a but for the 900 hPa level and divergence units of 10^{-6} g kg^{-1} s^{-1}; (c) same as Figure 2b but for the 700 hPa level. Below are the corresponding horizontal streamlines for (d) the vertically integrated moisture flux, (e) the 900 hPa level, and (f) the 700 hPa level. Point A (10°E, 22°N) at the center of the Sahara anticyclone is depicted in Figure 2d and further discussed in reference to Figure 3a.

relatively small divergence/convergence values which were discussed in section 3.

Examination of the horizontal moisture transport fields at isobaric levels shows much more intense circulation patterns. The streamlines at 900 hPa, Figure 2c, reveal convergence lines along 20°N from both northern/midlatitude sources and southwestern/tropical sources. These fluxes result in extended moisture convergence zones mainly over the central and southern parts of North Africa depicted in Figure 2b. At 700 hPa (Figure 2c), however, these zones turn out to be divergence zones, revealing the convective nature of this climate region, where the converged 900 hPa moisture ascends and diverges via the easterlies at 700 hPa. At the northern part of North Africa the relations between the 700 hPa and the 900 hPa reverse, where very weak convergence (inside the zero contour, i.e., 20°E, 25°N, and 0°E, 28°N) tops the 900 hPa divergence. This relation can be expected in this region characterized by the descending branch of the Hadley cell. Thus we can see that the relatively low vertically integrated $\nabla \cdot \mathbf{Q}$ over North Africa is a net result of integrating much more intense contributions from different altitudes. Consequently, if the vertical circulations, such as the Hadley cell, are smoothed in the assimilation, this will lead to a smoothed field of $\nabla \cdot \mathbf{Q}$, which might not represent well the local $E - P$ in these regions.

The three-dimensionality of the moisture transport is even more evident from the profiles of the terms of the three-dimensional moisture balance, (equation (3)). Figures 3a and 3b depict these profiles for two selected grid points, one at the center of the Saharan anticyclone shown in Figure 2d (point A at 10°E, 22°N) and the other at the maximum $\nabla \cdot \mathbf{Q}$ over the eastern Mediterranean shown in Figure 1d (point B at 30°E, 32°N), respectively. The dashed line in each of these figures is the horizontal moisture convergence, or minus divergence $(-\nabla \cdot \overline{q\mathbf{V}})$; that is, positive values act to increase the moisture content, and its vertical integrated value is the minus of $\nabla \cdot \mathbf{Q}$. Similarly, the dotted line is the vertical convergence $(-\partial \overline{q\omega}/\partial p)$, calculated off line from the assimilated vertical moisture flux on pressure levels. Its vertically integrated value should therefore be zero, and deviations from zero are only due to numerical errors in the calculation on pressure levels and not on the model's sigma levels. The solid line is the apparent moisture net source S_q, calculated as the residual in the moisture equation. The three lines therefore sum to zero at each isobaric level.

It should be emphasized that S_q includes not only the sub-grid and physical moisture processes but also the incremental analysis updates IAU(q) which correct for errors in these processes and in the transport terms as well. It also includes the vertical distribution of the contribution of the horizontal Shapiro filter and also filling of moisture from below to remove negative specific humidity. The GEOS-1 data set provides also diagnostic estimation for the moisture change due to turbulence (Turb$Q$), and due to moist processes (Moist$Q$), resulting from the model parameterizations. The *Helfand and Labraga* [1988] level 2.5 scheme is employed in order to model the vertical turbulent flux. The moist processes consist of large-scale precipitation processes, or supersaturation rain, and sub-grid convection modeled by the relaxed Arakawa Schubert (RAS) scheme of *Moorthi and Suarez* [1992]. There is also an adjustment for the reevaporation of falling rain modeled by a Kessler type scheme following *Sud and Molod* [1988]. The profiles of Turb$Q$ and Moist$Q$ are shown in Figures 3c and 3d for the A and B grid points, respectively. The surface evaporation E is equal to the vertical integration of Turb$Q$, while the precipitation P results from the vertical integration of Moist$Q$.

The vertical structure of the balance at the center of the Sahara point (Figure 3a) is clearly revealing the character of convection, but without precipitation. Moisture is horizontally converged at levels below ~800 hPa and diverges above. The vertical convergence term clearly redistributes the moisture by removing it from the lower levels to the upper levels. The residual moisture net source term is doing the same job and is comparable in magnitude to the vertical term. Thus sub-grid-scale convection might be a plausible interpretation of this term. Precipitation, if it had occurred, would have resulted in negative values at the upper levels, or moisture loss, as was indicated in many studies before [*Shay-El and Alpert*, 1991]. The vertically integrated value of S_q is, however, very close to zero (Figure 2a), which does not reveal the vigor dynamic nature of the moisture circulation illustrated here by these vertical profiles.

The parameterized contributions of turbulence (Turb$Q$) and moisture processes (Moist$Q$), for point A, which are shown in Figure 3c (note the different scale of the abscissa line), are indeed supporting of the above scenario. Moist$Q$ is very close to zero, indicating no precipitation, while Turb$Q$ indicates vertical moisture redistribution from levels below ~750 hPa to above. The values are somewhat larger than the residual S_q line in Figure 3a, and the maximum level is higher (500 hPa, in comparison to 600 hPa). This may be partly due to the numerical errors in the calculation of S_q as well as to the other contributions, i.e., the IAU(q), the filter, and the filling from below. These additional contributions, however, seem to be small, as shown by the overall good agreement of the sum of Turb$Q$ and Moist$Q$ with S_q (Figure 3a). This agreement is not surprising, since the Sahara has very little observations to create IAU(q) corrections, and therefore the moisture balance is expected to be mainly dependent on the model parameterizations and dynamics.

It is also interesting to note that the contributions from the parameterized moist processes at point A (i.e., Turb$Q$ and Moist$Q$) are not negligible in comparison with the dynamical terms. In fact, S_q in Figure 3a is of the same order as the large-scale horizontal and vertical transport. Hence even in this nonrainy region, $\nabla \cdot \mathbf{Q}$ is highly affected by the moist parameterizations, in particular the surface evaporation and its vertical turbulent transport, and not only by the dynamical transport. As mentioned before, some studies (applying the residual method) assume that $\nabla \cdot \mathbf{Q}$ calculated from an assimilated data set provides an indirect estimate of the "real" $E - P$, which does not rely on the parameterizations. Our findings however, show to the contrary, i.e., that $\nabla \cdot \mathbf{Q}$ in this region is largely a direct result of these parameterizations. Consequently, its interpretation as the net source must also be biased by the model deficiencies.

The vertical profile for the point of maximal $\nabla \cdot \mathbf{Q}$ in the eastern Mediterranean, as shown in Figure 1d (point B at 30°E, 32°N), is depicted in Figure 3b. Note again the different scale of the abscissa line compared with Figure 3a. The contributions to the strong horizontal advections are coming from levels below 800 hPa. Above these levels the moisture is blocked due to the strong subsidence, prevailing in summer. This subsidence is also shown by the vertical convergence line to damp moisture from the upper troposphere to the lower. The S_q line mainly reflects the evaporation from the sea surface and its sub-grid-scale vertical transport to the upper tro-

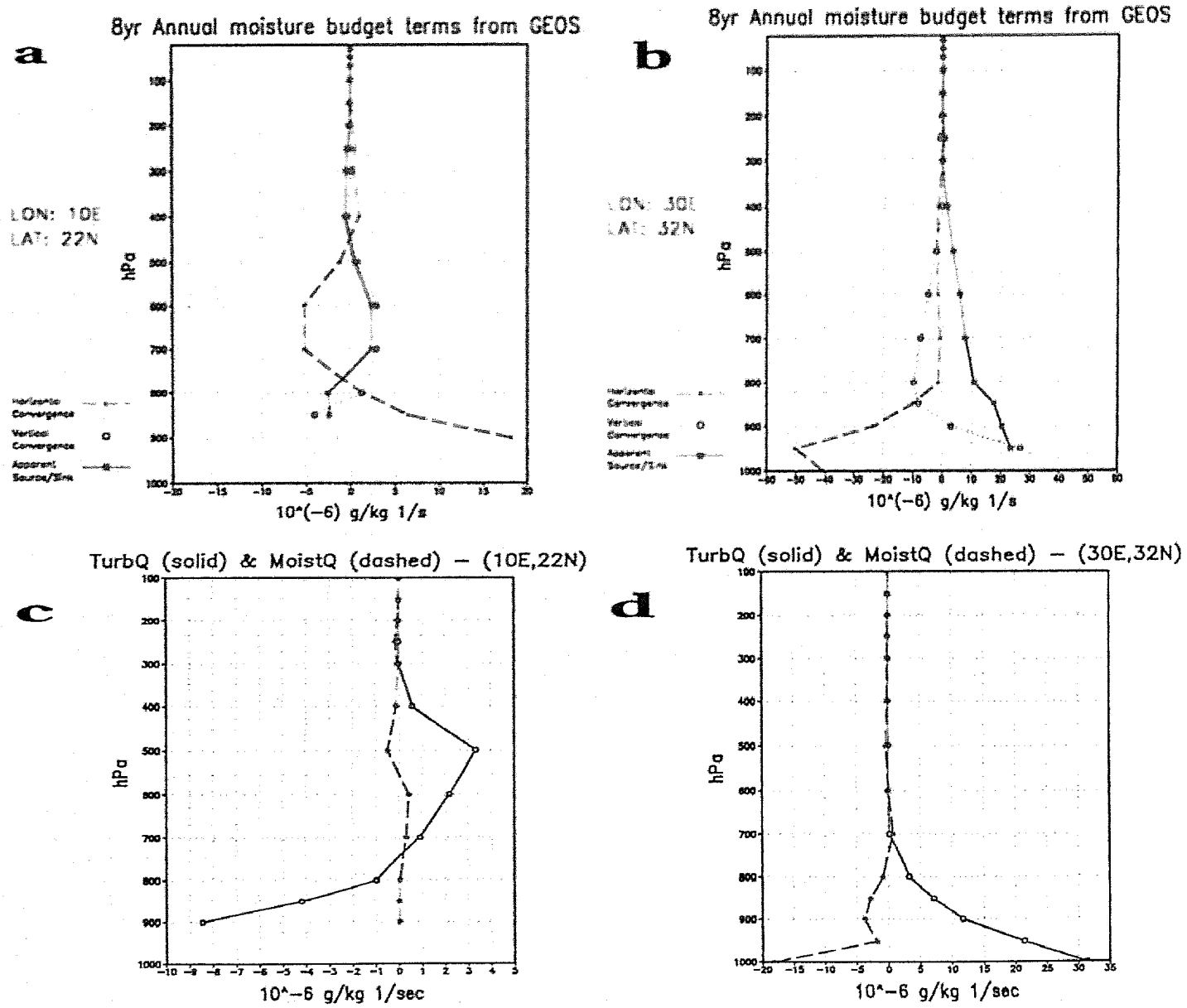

Figure 3. (a) Vertical profiles of the 8-year annual mean moisture budget terms, calculated from NASA/GEOS-1 data set, at point 10°E, 22°N (point A in Figure 2d), in the Sahara Desert. Horizontal convergence line is dashed, vertical convergence is dotted, and the apparent net source is solid. (b) Same as Figure 3a but at point 30°E, 32°N (point B in Figure 1d), in the eastern Mediterranean. (c) Same as Figure 3a but for the moisture change due to turbulence (Turb$Q$, solid line) and moist processes (Moist$Q$, dashed line). (d) Same as Figure 3c but for point B. All units are in 10^{-6} g kg^{-1} s^{-1}. Notice the different abscissa scales.

posphere. This region has considerable precipitation amounts (~0.5 mm/d, Figure 1b), thus the latent heat flux must be even stronger than the indicated S_q line. Indeed, Figure 3d is revealing a stronger Turb$Q$ at the levels below 700 hPa, while the precipitation drying effect, as evident from the negative Moist$Q$, is also limited below 700 hPa. The opposite acting forces in this region, of convection from the sea surface against a prevailing subtropical subsidence, are suggested to be uniquely large. This region is known to be an important moisture source for the Middle Eastern cyclones [*Alpert and Shay-El*, 1994]; however, it is also a source for the North African moisture, as was shown in Figure 2 and also discussed by *Alpert and Ziv* [1989] with reference to the Sharav cyclone that moves along the North African coast during the spring.

In section 5 we will study the area-averaged moisture flux divergence over the Sahara, focusing on the study area (10°W–30°E : 15°N–30°N), depicted in Figure 1d, following *Vitart et al.* [1996]. In Figure 4 (top) we show the annual mean streamlines of the vq and ωq averaged zonally over the study box 10°W–30°E. The averaged zonal component of the flux uq is shown in shadings. Noticeable are the strong low-level moisture flux into the Sahara from the midlatitudes at the northern boundary and from the tropics at the southern boundary. This flux is ascending at latitudes south of 24°N, while subsidence is evident at low levels at the 24°N–36°N latitudinal belt. The moisture transport streamlines also converge to the mean subtropical jet (36°N, 350 hPa). This flux, however, must be weak in these high altitudes. The zonal component is mainly negative at low levels over the study area latitudes (15°N–30°N), due to the easterlies, however it turns to positive values (westerlies) at higher altitudes. This is more evident in the East-West cross section of meridional mean moisture transport, along 15°N–30°N, shown in Figure 4 (bottom). The light shadings of the vq component is revealing that the core of the flux from the Mediterranean is on the eastern boundary (~30°E) near the surface. This flux flows westward, while ascending, and then turns eastward along a tilted line stretched from almost the surface at 35°E to ~550 hPa at the western boundaries (~0°E). The area-averaged divergence of the moisture flux is studied in the following section.

5. Area Averaged Moisture Flux Divergence over the Sahara

Vitart et al. [1996, p. 192] studied the hydrology of the North Africa desert by calculating the area-averaged $\nabla \cdot \mathbf{Q}$, based on NCEP data. They focused on the box between 10°W and 30°E longitude and 15°N and 30°N latitude, concluding that "the NCEP reanalysis over the North African dry regions confirm *Starr and Peixoto*'s [1958] result of an excess of evaporation over precipitation, even when diurnal variations are taken into account. However, more research is clearly needed to investigate the effects of gaps in upper air data, and possible contributions due to inflow or outflow of condensed water in clouds into the desert regions." In this section we will question this moisture source over the North African Sahara Desert, based on NASA reanalysis, and in particular we will show the dependency of the apparent source/sink on the size of the averaging box, and particularly on its proximity to the surrounding water bodies.

The averaging of $\nabla \cdot \mathbf{Q}$ in a box equals the outflow minus inflow through the boundaries, or

$$[\nabla \cdot \bar{\mathbf{Q}}]_{\text{box}} = \frac{(\overline{uq})_E - (\overline{uq})_W}{L_{W\text{-}E}} + \frac{(\overline{vq})_N - (\overline{vq})_S}{L_{N\text{-}S}} \qquad (4)$$

where the right-hand side (RHS) terms are vertically integrated, and E, W, N, S subscripts stand for East, West, North, and South boundaries, respectively. L stands for the average distance between the boundaries. The calculation of the area average took into account the change of the grid size in longitude and latitude (through the "area-average" function as defined in the grids analysis and display system, i.e., GrADS [e.g., *Doty*, 1995]). Figure 5 (top) shows the meridional average of the vertically integrated uq along the latitudinal belt of 15°–30°N, as function of the longitude. The average flux is eastward at longitudes east of ~18°E and westward west of this longitude. The first term on the RHS of (4), or the contribution of the East-West flux to the divergence, is proportional to the difference of these fluxes between any two longitudes. In particular, the box of *Vitart et al.* [1996] is marked on the figure by the vertical lines at 30°E and at 10°W. The resulting contribution to the area-averaged divergence is positive because of the out flux at the eastern boundary, and at the western boundary as well, hence $(uq)_E - (uq)_W > 0$. It is interesting to note that the slope of the line is increasing near the eastern and western boundaries of the continent, probably due to the low-moisture contents at the center of the Sahara Desert. This already hints that the area-averaged divergence depends on the dimensions of the box and its location relative to the continent's boundaries.

Similarly, Figure 5 (bottom) depicts the vq flux averaged between the 10°W longitude and the 30°E longitude. The flux north of 10°N is negative, indicating that the average meridional flux is from the north. The flux is becoming increasingly negative until 30°N, indicating that the North-South contribution to the divergence, or the second term on the RHS of (4), is negative. Combining the pictures of both Figures 5 (top) and 5 (bottom), we see that the flux converges over North Africa through the northern and southern boundaries and diverges through the eastern and western boundaries.

The dependency of the divergence on the location of the northern boundary is studied in Figure 6a, showing the area-averaged $\nabla \cdot \mathbf{Q}$ in a box bounded at the west by 10°W longitude, at the east by 30°E longitudes, at the south by 15°N, but with by a variable latitude at the north. The purpose of this is to explore the potential moisture flux contribution from the Mediterranean. The average divergence is always positive; however, it decreases when the northern boundary is between 19°N and 27°N, indicating again that the divergence bands are located more on the southern and northern boundaries, which are closer to the water sources. Similarly, Figure 6b is with a variable eastern boundary. The main feature in this figure is the steep slope at longitudes west of 6°E, indicating the zone of influence of the Atlantic Ocean. The distance of the western boundary (10°W) from the Atlantic Ocean varies between ~100 and 400 km. The steepest slope is at about 2°W (or about 900–1200 km). The sea breeze may account for up to 200–300 km, but moisture diffusion over 3–4 grid points ($\Delta x = 2.5°$) may explain this distance. Both figures have minimum when the moving boundary is at about the center of the Sahara Desert, associated with the convergence at the middle of the Sahara which is surrounded by regions of divergence. This point is further illustrated in Figure 6c, showing the area-averaged $\nabla \cdot \mathbf{Q}$ in an expanding box centered on 10°E, 22.5°N. This is the central point in the Sahara box in the study of *Vitart*

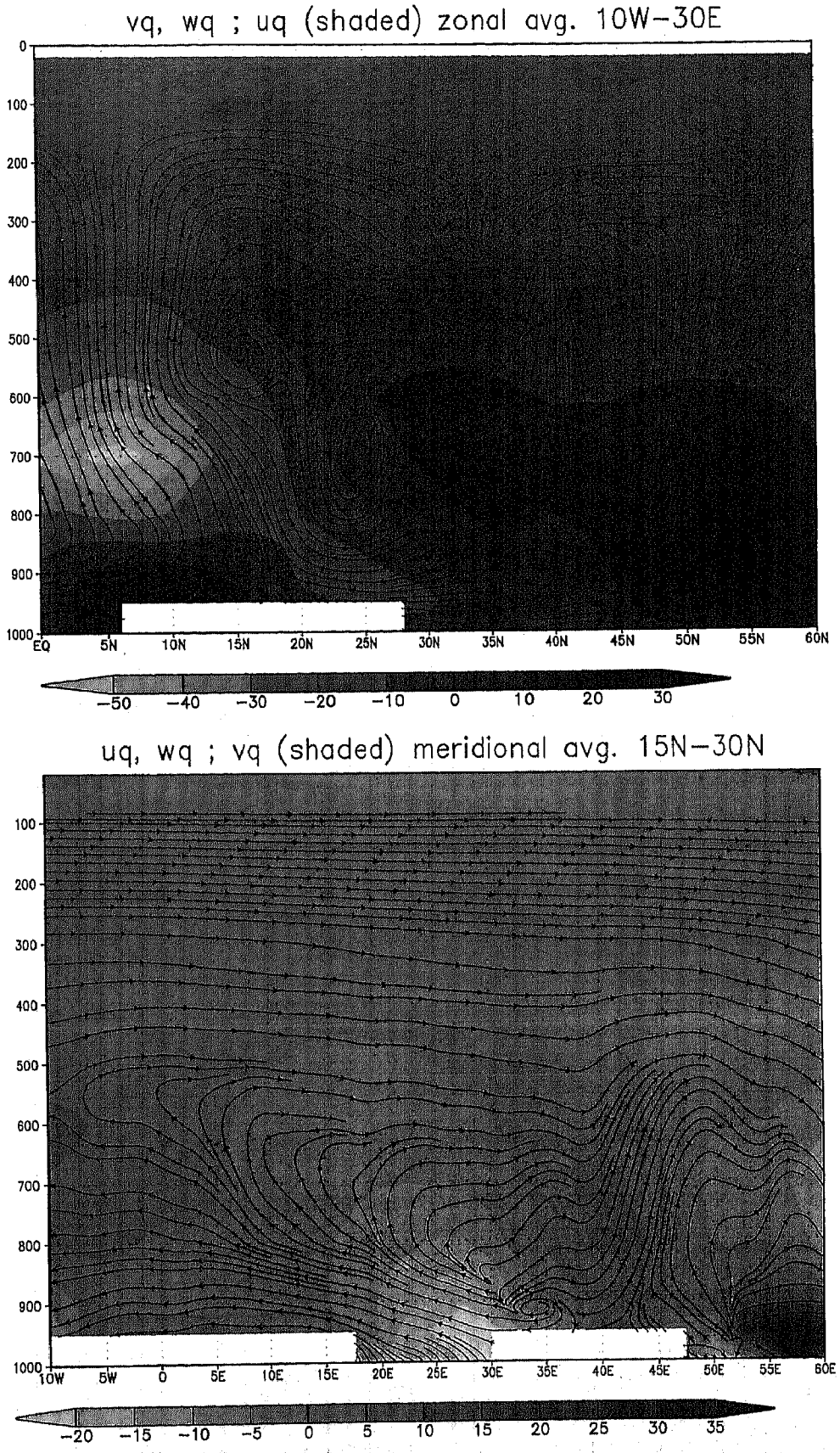

Figure 4. (top) Vertical crossection of the 8-year mean moisture streamlines (vq, ωq), zonally averaged for 10°W–30°E, and uq in shadings, calculated from NASA/GEOS-1 data set. (bottom) Same as Figure 4 (top) but for uq-ωq streamlines, averaged meridionally along 15°N–30°N, with vq in shadings. A shading bar, in units of 10^{-6} g kg^{-1} s^{-1}, is at the bottom of each figure.

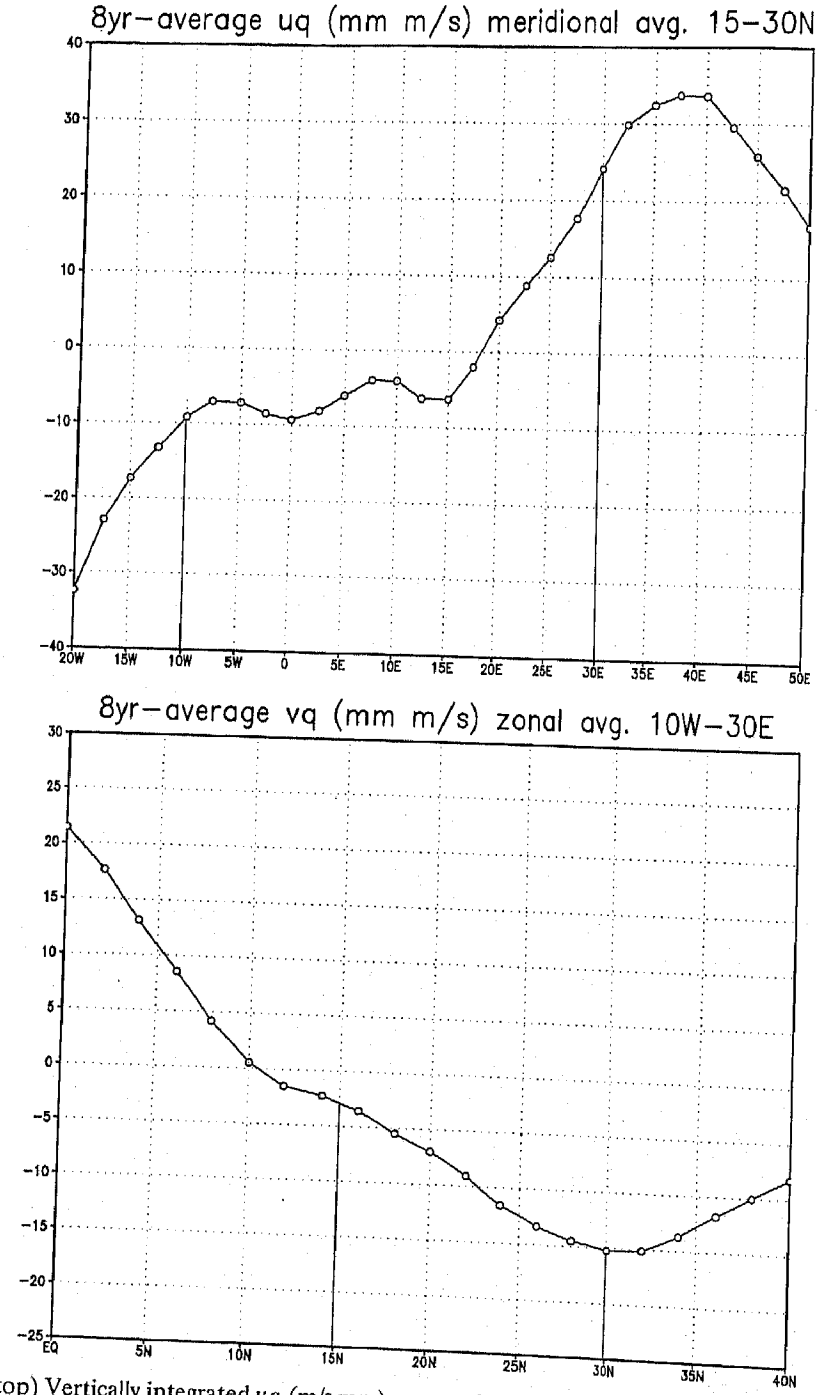

Figure 5. (top) Vertically integrated uq (m/s mm), averaged meridionally along 15°N–30°N, based on 8-year means of NASA/GEOS-1. The vertical lines at 30°E and at 10°W indicate the boundaries of the Sahara box chosen by *Vitart et al.* [1996]. (bottom) Same as Figure 5a but for vq, averaged zonally along 10°W–30°E. Boundaries of the box are indicated by vertical lines at 15°N and 30°N.

et al. [1996]. In each expansion step the box is expanded by 4° longitude and 1.5° latitude, corresponding to the elongated rectangular shape of North Africa. Thus, for example, step 10 matches the box of *Vitart et al.* [1996], i.e., 10°W–30°E : 15°N–30°N, with averaged divergence value of 0.18 mm/d, in good agreement with the 0.20 mm/d obtained by *Vitart et al.* [1996] using NCEP reanalysis.

Figure 6c shows that if the averaging area is not too big, i.e., expansion step less than 6, the North African Desert can be classified as a convergence zone, because the values of the integrated moisture divergence are negative. This suggests that if the averaging box is big enough to include the boundaries of the continent, only then can it be classified as a divergence zone. The curve grows smoothly with the expansion steps, thus it may indicate that the hypothetical divergence may be only due to the large-scale smoothed water/land transition between the surrounding subtropical water bodies and the dry desert. In particular, there is an increase in the slope of the curve at step

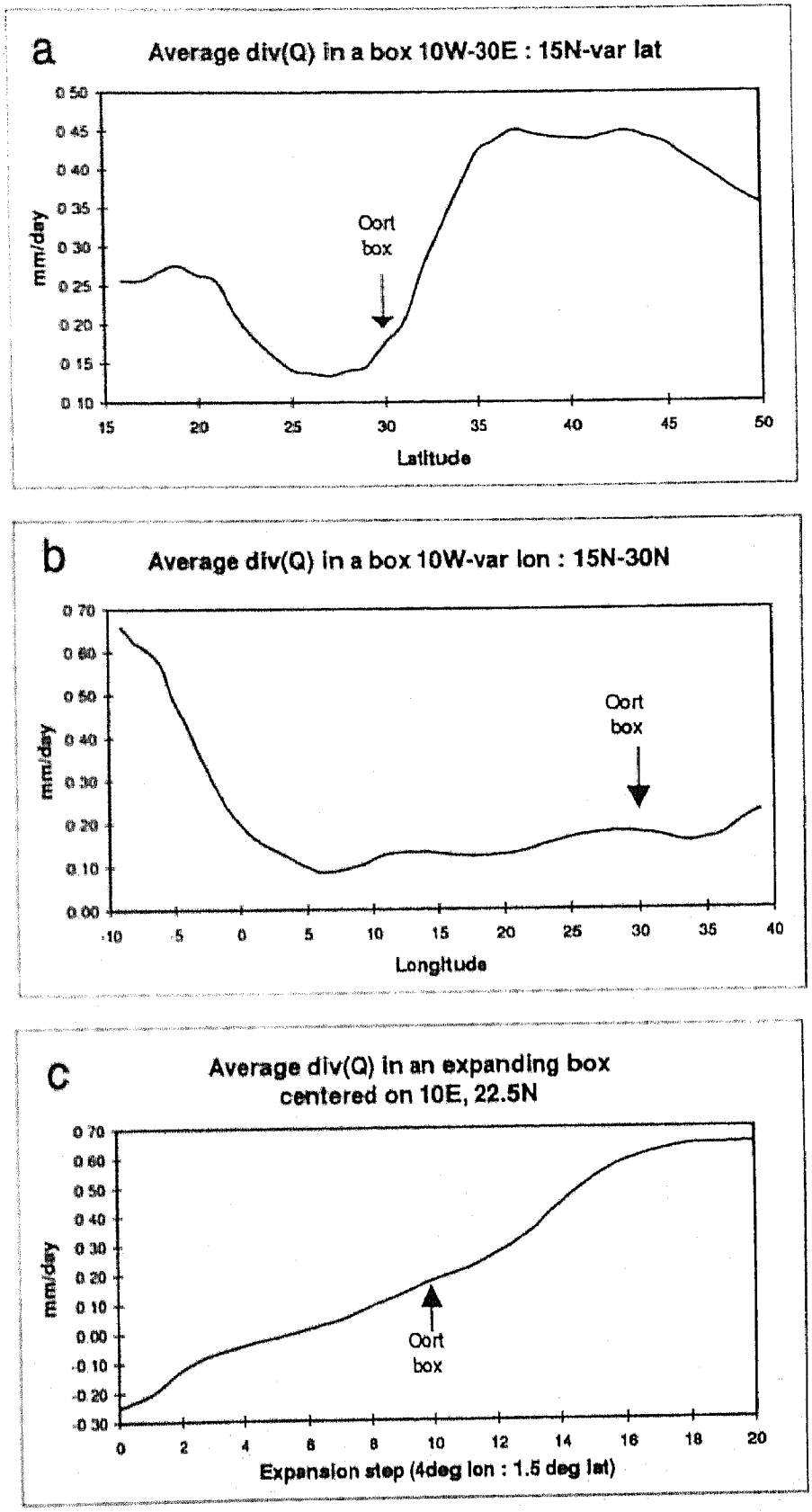

Figure 6. Area-averaged moisture flux divergence in a box over the Sahara: (a) with a movable northern boundary (10°W–30°E : 15°N-varied northern latitude); (b) with a movable eastern boundary (10°W-varied eastern longitude : 15°N–30°N); (c) in an expanding box centered on 10°E, 22.5°N. In each expansion step, the box is expanded by 4° longitude and 1.5° latitude. Oort box (10°W–30°E : 15°N–30°N), following *Vitart et al.* [1996], is indicated by the arrows. All divergence values are based on 8-year means of NASA/GEOS-1.

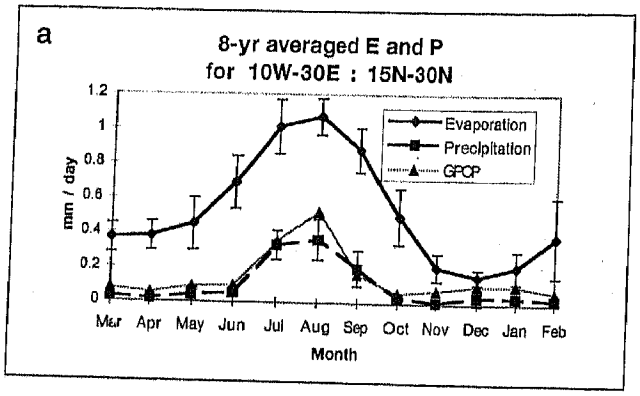

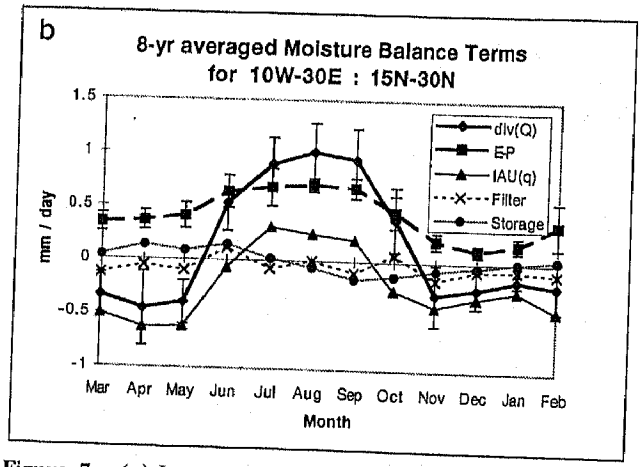

Figure 7. (a) Intermonthly variability of evaporation E and precipitation P, in mm/d, averaged for the "Oort" Sahara box (10°W–30°E : 15°N–30°N), based on 8-year means of NASA/GEOS-1 and 7-year mean precipitation from GPCP satellite-gauge estimation [*Huffman et al.*, 1997]. Error bars for E and P are standing for ±1 standard deviation of the interannual variability, calculated from the 8 yearly values. (b) As in Figure 7a but for the NASA/GEOS-1 moisture balance terms: $E - P$, $\nabla \cdot \mathbf{Q}$, IAU(q), storage(q), and Shapiro filter (see legend for line markings).

12, i.e., box of 14°W–34°E : 13.5°N–31.5°N, which is the best description of the coastlines of the continent using this expanded box symmetry. These results therefore question the classification of the North African Desert as divergence zone and suggest that the net-averaged divergence may be due to smoothing effects. The smoothing can be caused by physical diffusive processes, i.e., the sub-grid-scale fluxes, or the diurnal variation of the breeze [e.g., *Vitart et al.*, 1996], or the intrusion and evaporation of clouds (e.g., Y. Shay-El et al., 1998), and it can be partly explained also by the low resolution of the model and the observational cover.

6. Intra-annual Variability and Model Biases

Inspection of the intermonthly variability and the diurnal variability of the moisture balance terms can shed some light on the nature of the smoothing processes. Figure 7a depicts the intermonthly variability of the 8-year means of E and P averaged for the Sahara box. Error bars are standing for ±1 standard deviation of the interannual variability, calculated for each month from the 8 yearly values. As mentioned earlier, E and P are primarily diagnostic fields created by the model's parameterizations and are therefore merely an estimation of the real evaporation and precipitation. For comparison, Figure 7a depicts also the 7-year (July 87 to June 94) mean precipitation over this area from the satellite-gauge analysis of GPCP (Global Precipitation Climatology Project) [*Huffman et al.*, 1997]. This estimation is the main product of a merged analysis incorporating several precipitation estimates from low-orbit-satellite microwave data, geosynchronous-orbit-satellite infrared data, and rain gauge observations. The P estimation, from the reanalysis, seems to quite agree with the GPCP, although it is somewhat underestimated for all months except September.

The averaged evaporation in Figure 7a is larger than the precipitation for the whole year. Both have maximum at August. The precipitation maxima is due to some tropical contribution in the southern part of the box, while the evaporation is contributed more in the northern part of the box, close to the Mediterranean. The error bars are not large, compared to the seasonal variability, meaning that this cycle is significant.

Similarly, Figure 7b depicts the intermonthly variability of the 8-year means of the moisture balance terms averaged for the Sahara box. The terms included are $E - P$, and $\nabla \cdot \mathbf{Q}$, as well as the increments IAU(q), the storage ($\partial q/\partial t$), and the Shapiro filter computed as the residual in the balance. The differences between the two curves of $E - P$ and $\nabla \cdot \mathbf{Q}$ are mainly due to the contribution of the IAU, and they mainly represent the biases in the model's $E - P$ and the missing physical processes in the assimilation moisture balance. The contributions of the storage and the filter are relatively small compared to the other terms. While $E - P$ is positive all year-around, $\nabla \cdot \mathbf{Q}$ is negative for the 7-month period between November and May, meaning that the region is a moisture sink and not a source during these months. Both $E - P$ and $\nabla \cdot \mathbf{Q}$ have a maximum during the summer; however, the amplitude of the seasonal variability of $\nabla \cdot \mathbf{Q}$ is larger than that for $E - P$. The annual mean $\nabla \cdot \mathbf{Q}$ of 0.18 mm/d is relatively small compared to the seasonal amplitude of about 0.75 mm/d (defined as half of the maximum variability between April and August) and is about the order of the error bars. This strengthens the question to what extent this annual net moisture source is significant.

Figure 8 depicts the diurnal variability of $\nabla \cdot \mathbf{Q}$ and $E - P$, similarly to Figure 7b. The error bars, depicted only for $\nabla \cdot \mathbf{Q}$,

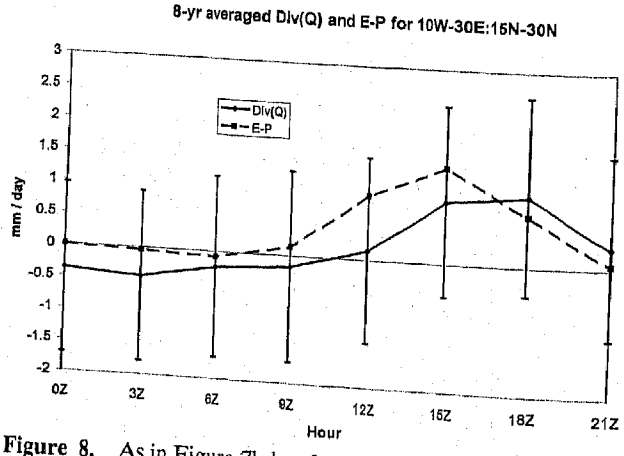

Figure 8. As in Figure 7b but for a diurnal variability of $E - P$ and $\nabla \cdot \mathbf{Q}$ terms. Error bars are marked only for $\nabla \cdot \mathbf{Q}$ and represent the standard deviation for each hour based on ~2920 (8 years × 365 days) daily values.

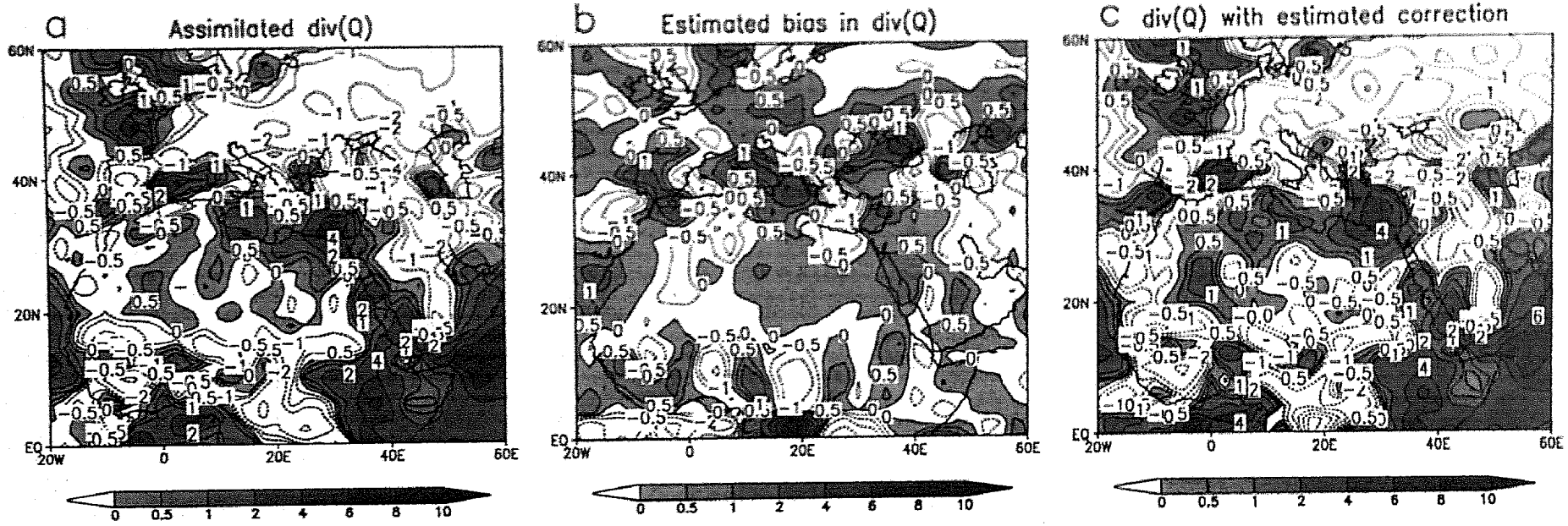

Div(Q) with estimated bias correction for Jan 1987

Figure 9. (a) Averaged $\nabla \cdot Q$, as in Figure 1d, but only for January 1987. (b) Estimated model bias in $\nabla \cdot Q$ for January 1987, calculated as "first guess − analysis." (c) $\nabla \cdot Q$ with estimated bias correction for January 1987. Contour and shadings as in Figure 1.

represent the standard deviation based on the ~2920 daily values. Hence they represent the daily-scale variability as well as the interannual variability and are therefore much larger than the error bars in Figure 7. $E - P$ has a maximum at the late afternoon 1500 UT and is very close to zero between 2100 and 0900 UT. $\nabla \cdot \mathbf{Q}$ shows, however, negative values between 0000 and 0900 UT (it also approximately represents the local time; see next paragraph), designating convergence during these hours. *Vitart et al.* [1996] showed that this convergence is contributed more at the southern subbox, of 15°–20°N. In the same way as for the monthly variability, the diurnal mean value is smaller than the amplitude of the diurnal cycle and of the error bars, thus weakening the net positive source argument.

The diurnal cycle of $\nabla \cdot \mathbf{Q}$ seems to lag by ~3 hours behind the $E - P$ cycle. Such a time shift may be expected, following a simplified theory of diurnal boundary layer oscillations in the presence of weak turbulent damping [e.g., *Paegle and McLawhorn*, 1983]. This theory allows for a ~3- to 6-hour time shift of the maximum response of such oscillations equatorward of 30° latitude. The NASA reanalysis may be mimicking this theoretical result over the Sahara. This indicates again that $\nabla \cdot \mathbf{Q}$ in this region is largely a response to the $E - P$ forcing.

It is also interesting to note that the diurnal cycle of $\nabla \cdot \mathbf{Q}$ is in the opposite direction to a cycle that can be expected over land from the diurnal sea breeze cycle. It is expected that during daytime there will be a moisture flux at lower levels from the surrounding water bodies into the dry land atmosphere, while the upper levels return flow will be weaker, resulting in a net moisture convergence, and similarly a net moisture divergence at nighttime. Nevertheless, such a signal, if existing, seems to be smaller in magnitude than the more prominent $E - P$ forcing.

As mentioned above, the differences between the $E - P$ and the $\nabla \cdot \mathbf{Q}$ fields are contributed by the IAU of the specific humidity (q), calculated from the differences between analyzed q and first guess q, which is inserted into the assimilation as an additional forcing in the moisture equation. This IAU is correcting the balance for the total errors in the moisture fields. It is unknown, however, to what extent these mean errors, or biases, are contributed from the physical $E - P$ term, or from the dynamical $\nabla \cdot \mathbf{Q}$ term. The biases of the $\nabla \cdot \mathbf{Q}$ term can be estimated by the differences between the analyzed $\nabla \cdot \mathbf{Q}$ and the first guess $\nabla \cdot \mathbf{Q}$. Figure 9a is showing, for instance, the monthly mean $\nabla \cdot \mathbf{Q}$ for January 1987, from NASA's assimilation. The divergences were also calculated by using the first guess (model forecast) wind and specific humidity, yielding a first-guess estimation of $\nabla \cdot \mathbf{Q}$. Similarly, an estimation of the analyzed $\nabla \cdot \mathbf{Q}$ was done using the fields saved after the optimal interpolation step. Both these divergences were vertically integrated on pressure levels and are time averaged using the instantaneous wind and moisture fields saved every 6 hours. Unlike these, the assimilated mean $\nabla \cdot \mathbf{Q}$ is integrated during the assimilation model run, i.e., on sigma levels and every time step. Nevertheless, the first-guess divergence minus the analysis divergence, depicted in Figure 9b, can still provide a useful estimation for the bias in the divergence. Fortunately, this difference field is smaller than the assimilated divergence over most areas, thus it limits the uncertainty in the moisture flux divergence. However, over North Africa it is about the order of the assimilated divergence. This means that we cannot take for granted that the errors in the assimilation moisture balance are only due to the parameterized $E - P$. Errors, or uncertainties, are also included in the $\nabla \cdot \mathbf{Q}$ field, and therefore their estimation is essential for significant calculation of the moisture net source/sink based on the divergence.

Dee and da Silva [1998] have shown that forecast biases are not removed during the assimilation. Therefore the $\nabla \cdot \mathbf{Q}$ from the assimilation is closer to the $\nabla \cdot \mathbf{Q}$ from the model's first guess, more than to that from the analyzed observations. They have suggested a method for on-line estimation and correction of these forecast biases. This method, however, is not yet implemented in GEOS-1/DAS. The correction to the assimilated $\nabla \cdot \mathbf{Q}$ can be roughly estimated from the off-line fields, by subtracting the first guess minus analysis bias depicted in Figure 9b. The resulting "corrected" $\nabla \cdot \mathbf{Q}$ is shown at Figure 9c. Noticeable differences between Figures 9a and 9c are the extended convergence zones in the central eastern parts of the Sahara. The Sahara (negative values) and the enhanced divergence in the northern part of the Sahara. The area average of the assimilated $\nabla \cdot \mathbf{Q}$ in the Sahara box for January 1987 is −0.0705 mm/d, the average of the estimated bias is −0.0790 mm/d, leading to an estimated "corrected" $\nabla \cdot \mathbf{Q}$ of 0.0085 mm/d. Hence the divergence in this region may even change sign with proper handling of the forecast bias. This point illustrates again that the classification of North Africa as a moisture source or sink is still below the level of a robust decision. Over the Arabian-Iraqi desert the bias correction does not seem to change significantly the net sink pattern.

7. Summary and Conclusions

The complex three-dimensional large-scale in/out moisture transport to the Sahara, which was discussed in the previous sections, is somewhat simplified in Figure 10. This figure sketches by arrows the moisture fluxes at the boundaries of two vertically aligned boxes over our Sahara study domain. The arrows in the bottom box represent the horizontally integrated flux through the boundaries, integrated vertically from the surface up to 800 hPa isobaric level. The top box is similarly from 800 hPa up to the 10 hPa top level. The fluxes depicted are the 8-year annual averages in 10^6 kg/s units. The 800 hPa is the level separating between moisture convergence at lower levels (bottom box) and divergence above. The vertical dashed

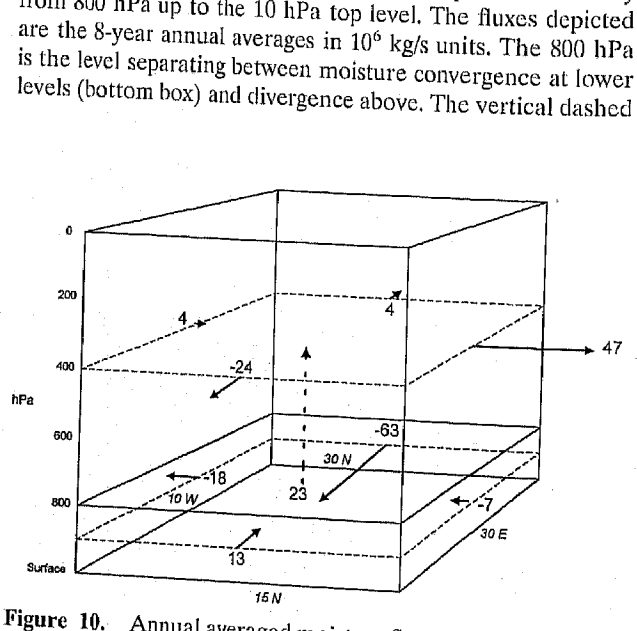

Figure 10. Annual averaged moisture flux arrows (in 10^6 kg/s units) integrated at the boundaries of two vertically aligned boxes over the Sahara (10°W–30°E : 15°N–30°N), separated by 800 hPa level. Vertical dashed arrow represents the vertical flux at 800 hPa (for more details see text).

Table 1. Integrated Moisture Balance Terms Over the Sahara Box (10°W–30°E : 15°N–30°N) in 10^6 kg/s Units (1 mm/d = 79 × 10^6 kg/s)

	$\nabla \cdot Q$				
Layer	$\nabla \cdot Q$ = Turb$Q$	+Moist$Q$	+IAU(q)	$-\omega q_{800}$	$+\varepsilon$
800–10 hPa	71	77	−3	−21	23	−5
Surface to 800 hPa	−65	−40	−5	3	−23	0
Surface to 10 hPa	6	37	−8	−18	0	−5

The moisture flux divergence ($\nabla \cdot Q$) is the sum of the five columns to its right: turbulence (Turb$Q$), moist processes (Moist$Q$), incremental analysis updates (IAU(q)), vertical flux at 800 hPa ($-\omega q_{800}$), and residual error (ε).

arrow represents the vertical flux at 800 hPa, from the bottom box to the top one, also in 10^6 kg/s units. The stronger inflow is from the Mediterranean (the 30°N northern boundary) at the bottom box (63 × 10^6 kg/s), while the stronger outflow is due to the subtropical jet at the eastern boundary (30°E), at the top box (47 × 10^6 kg/s).

This is further illustrated in Table 1, which summarizes the integrated values of the balance terms for the two-layered Sahara boxes, based on NASA/GEOS-1 reanalysis. The $\nabla \cdot Q$ column is the sum of all the five columns to its right. The terms Turb$Q$, Moist$Q$, and IAU(q) are the moisture contributions due to turbulence, moist processes, and analysis updates, respectively, while $-\omega q_{800}$ is the vertical flux at 800 hPa from the lower layer to the upper one, and ε is the residual error partly due to other smaller terms (Shapiro's filter in particular) and partly due to various numerical errors in calculations. (The numerical errors are associated with the following reasons: (1) Some terms are given on sigma levels while other on pressure; (2) fluxes are "snapshots" at analysis times, while diagnostics are averaged for every time step; (3) use of different integration schemes on-line and off-line.) Most important to note is that the column-integrated net divergence (6 × 10^6 kg/s = 0.08 mm/d) is 1 order smaller than the divergence in the upper layer (71 × 10^6 kg/s) and convergence in the lower layer (−65 × 10^6 kg/s) and is about the order of the error. This column-averaged divergence value is also smaller than the 0.18 mm/d value calculated before from the diagnostic vertically integrated fluxes, which are summed every time step. This further illuminates the uncertainties involved in the classification of the North African Sahara Desert as net moisture source or sink. It is also interesting to note that the observation corrections IAU(q) act mostly to decrease the moisture in the upper layer, which is probably due to excessive evaporation in the model.

For conclusion, two major findings are as follows:

First, considering the temporal and spatial variability and the relative lack of observations, the classification of the North African Sahara Desert as a net moisture source might be still below a robust detectable level.

Second, the vertically integrated moisture flux converges at the center of North Africa, while divergence bands are located near the boundaries of the continent, close to the surrounding water bodies. This suggests that the finding of a net source results from smoothing the water/land boundary. This smoothing, much due to the coarse model resolution and sparse observations, is certainly also affected by real atmospheric diffusion processes such as the sea breeze cycle, as well as cloud intrusion and evaporation. A similar conclusion was reached by *Trenberth and Guillemot* [1998] who attributed such phenomena to the "ringing effect" of the surrounding seas at finite spectral model resolution.

Following these findings it is suggested that averaging over the North African Sahara Desert in a box may not be sufficient for studying the hydrological cycle of this nonhomogeneous area. Further local observations and mesoscale studies are required, in particular high-resolution modeling of the sea breeze and the associated coastal processes like cloud formation.

Acknowledgments. Special thanks go to the Data Assimilation Office at NASA Goddard for the data and support. P. Alpert was NRC associateship visitor at Goddard while most of the work was done.

References

Alpert, P., and B. Ziv, The Sharav cyclone—Observations and some theoretical considerations, *J. Geophys. Res.*, *94*, 18,495–18,514, 1989.

Alpert, P., and Y. Shay-El, The paradox of the winter net moisture sink over the Arabian-Iraqi desert, *Ann. Geophys.*, *11*, 190–194, 1993.

Alpert, P., and Y. Shay-El, The moisture source for the winter cyclones in the eastern Mediterranean, *Israel Meteorol. Res. Pap.*, *5*, 20–27, 1994.

Alpert, P., Y. Shay-El, and A. da Silva, Moisture sinks/sources over the Mediterranean and Arabia/Iraqi desert (Preprint), paper presented at the 2nd International Scientific Conference on the Global Energy and Water Cycle, World Clim. Res. Program, June 17–21, Washington, D. C., 1996.

Alpert, P., H. Shafir, and D. Issahary, Recent changes is the climate at the Dead Sea—A preliminary study, *Clim. Change*, *37*, 513–537, 1997.

Atkinson, B. W., *Meso-scale Atmospheric Circulations*, 495 pp., Academic, San Diego, Calif., 1981.

Bloom, S. S., L. L. Takacs, A. M. da Silva, and D. Ledvina, Data assimilation using incremental analysis updates, *Mon. Weather Rev.*, *124*, 1256–1271, 1996.

da Silva, A., and G. White, A Comparison of surface marine fluxes from GEOS-1/DAS and NMC reanalyses, in *Proceedings of the Workshop on the GEOS-1 Five-Year Assimilation*, vol. 7, *NASA Tech. Memo. 104606*, pp. 129–136, 1995.

Dee, D. P., and A. da Silva, Data assimilation in the presence of forecast error bias, *Q. J. R. Meteorol. Soc.*, in press, 1998.

Doty, B., 1995: *The Grid Analysis and Display System-GrADS*, 148 pp., Cent. for Ocean-Land-Atmos. Stud., Calverton, Md., 1995. (http://grads.iges.org/grads/head.html)

Gibson, J. K., A. Hernandez, P. Kallberg, A. Nomura, E. Serrano, and S. Uppala, The ECMWF re-analysis project (Preprints), *Am. Meteorol. Soc.*, *10*, 288–291, 1994.

Helfand, H. M., and J. C. Labraga, Design of a non-singular level 2.5 second-order closure model for the prediction of atmospheric turbulence, *J. Atmos. Sci.*, *45*, 113–132, 1988.

Helfand, M., Schubert, S. D., and C. Y. Wu, Climatology and interannual variability of the great plains low level jet as assimilated by the GEOS-1 data assimilation system (Preprints), paper presented at the *GEWEX Symposium*, Global Energ. and Water Cycle Exp., Washington, D. C., 17–21 June, 1996.

Huffman, G. J., R. F. Adler, P. Arkin, A. Chang, R. Ferraro, A. Gruber, J. Janowiak, A. McNab, B. Rudolf, and U. Schneider, The Global Precipitation Climatology Project (GPCP) combined precipitation data set, *Bull. Am. Meteorol. Soc.*, *78*, 5–20, 1997.

Kalnay, E., et al., The NCEP/NCAR 40-year reanalysis project, *Bull. Am. Meteorol. Soc.*, *77*, 437–471, 1996.

Moorthi, S., and M. J. Suarez, Relaxed Arakawa Schubert: A parameterization of moist convection for general circulation models, *Mon. Weather Rev.*, *120*, 978–1002, 1992.

Oort, A. H., and J. P. Peixoto, Global angular momentum and energy balance requirements from observations, *Adv. Geophys.*, *25*, 335–490, 1983.

Paegle, J., and D. W. McLawhorn, Numerical modeling of diurnal convergence oscillations above sloping terrain, *Mon. Weather Rev.*, *111*, 67–85, 1983.

Peixoto, J. P., On the global water vapor balance and the hydrological cycle, in *Tropical Meteorology in Africa*, pp. 232–243, Munitalp Foundation, Nairobi, 1960.

Peixoto, J. P., Atmospheric vapor flux computations for hydrological purposes, *WMO Pub. 357*, World Meteorol. Organ., 83 pp., Geneva, 1993.

Peixoto, J. P., and A. H. Oort, *Physics of Climate*, 520 pp., Am. Inst. of Phys., New York, 1992.

Rasmusson, E. M., E. H. Berbery, C. F. Ropelewski, and E. S. Yarosh, An integrated strategy for the evaluation of GCIP continental-scale land/atmosphere moisture budgets (Preprint), paper presented at the 2nd International Scientific Conference on the Global Energy and Water Cycle, WCRP, June 17–21, Washington, D. C., 93–94, 1996.

Schemm, J., S. Schubert, J. Terry, and S. Bloom, Estimates of monthly mean soil moisture for 1979–1989, *NASA Tech. Memo. 104571*, 1992.

Schubert, S., R. Rood, and J. Pfaendtner, An assimilated data set for Earth Sciences applications, *Bull. Am. Meteorol. Soc.*, *74*, 2331–2342, 1993.

Schubert, S., C.-K. Park, C.-Y. Wu, W. Higgins, Y. Kondratyeva, A. Molod, L. Takacs, M. Seablom, and R. Rood, A multiyear assimilation with the GEOS-1 system: Overview and results, *NASA Tech. Memo. 104606*, vol. 6, 1995.

Shapiro, R., Smoothing, filtering and boundary effects, *Rev. Geophys.*, *8*, 359–387, 1970.

Shay-El, Y., and P. Alpert, A diagnostic study of winter diabatic heating in the Mediterranean in relation to cyclones, *Q. J. R. Meteoroll. Soc.*, *117*, 715–747, 1991.

Starr, V. P., and J. P. Peixoto, On the global balance of water vapor and the hydrology of deserts, *Tellus*, *10*, 189–194, 1958.

Sud, Y. C., and A. Molod, The roles of dry convection, cloud-radiation feedback processes and the influence of recent improvements in the parameterization of convection in the GLA GCM, *Mon. Weather Rev.*, *116*, 2366–2387, 1988.

Takacs, L. L., A. Molod, and T. Wang, Documentation of the Goddard Earth Observing System (GEOS) General Circulation Model—Version 1, *NASA Tech. Memo. 104606*, vol. 1, 1994.

Trenberth, K. E., and C. J. Guillemot, Evaluation of the global atmospheric moisture budget as seen from analysis, *J. Clim.*, *8*, 2255–2272, 1995.

Trenberth, K. E., and C. J. Guillemot, Evaluation of the atmospheric moisture and hydrological cycle in the NCEP/NCAR reanalyses, *Clim. Dyn.*, *14*, 213–231, 1998.

Vitart, F., A. H. Oort, and K. Mo, New results on the hydrology of the North African desert, based on the NMC reanalysis, in *Proceedings of the 20th Climate Diagnostics Workshop*, pp. 191–194, U.S. Dep. of Comm./NOAA/NWS, 1996.

Wang, M., and J. Paegle, Impact of analysis uncertainty upon regional atmosphere moisture flux, *J. Geophys. Res.*, *101*, 7291–7303, 1996.

P. Alpert and Y. Shay-El, Dep. of Geophysics and Planetary Sciences, Tel Aviv Univ., Israel 69978. (e-mail: yuval@cyclone.tau.ac.il)

A. da Silva, Data Assimilation Office, Code 910.3, NASA/GSFC, Greenbelt, MD 20771.

(Received March 24, 1998; revised August 25, 1998; accepted August 27, 1998.)